SCIENCE CHINA
Technological Sciences

• Article •

February 2018 Vol.61 No.2: 219–231
https://doi.org/10.1007/s11431-017-9121-6

# Experimental study on the new type of electrical storage heater based on flat micro-heat pipe arrays

WANG ZeYu[1], DIAO YanHua[1,2], ZHAO YaoHua[1,2*], LIANG Lin[1] & WANG TengYue[1]

[1] *Beijing Key Laboratory of Green Built Environment and Efficient Technology, Beijing University of Technology, Beijing 100124, China;*
[2] *Beijing Advanced Innovation Center for Future Internet Technology, Beijing 100124, China*

Received June 25, 2017; accepted August 16, 2017; published online September 13, 2017

A new type of electrical storage heater that utilizes latent heat storage and flat micro-heat pipe arrays (FMHPAs) was developed. The thermal characteristics of the heater were tested through experimentation. The structure and operating principle of the storage heater were expounded. Three rows of FMHPAs were applied (three rows with five assemblies each) with a mass of 28 kg of phase change material (PCM) in the heat storage tank. Electric power was supplied to the PCM in the range of 0.2–2.04 kW, and air was used as heat transfer fluid, with the volume flow rate ranging from 40–120 $m^3$/h. The inlet temperature was in the range of 15–24°C. The effects of heating power, air volume flow rate, and inlet temperature were investigated. The electrical storage heater exhibited efficiencies of 97% and 87% with 1.98 and 1.30 kW of power during charging and discharging, respectively. Application of the proposed storage heater can transfer electricity from peak periods to off-peak periods, and the excess energy generated by wind farms can be stored as heat and released when needed. Good economic and environmental benefits can be obtained.

**flat micro-heat pipe, latent heat storage, electrical storage heater, peak load shifting, wind power utilization**

**Citation:** Wang Z Y, Diao Y H, Zhao Y H, et al. Experimental study on the new type of electrical storage heater based on flat micro-heat pipe arrays . Sci China Tech Sci, 2018, 61: 219–231, https://doi.org/10.1007/s11431-017-9121-6

## 1 Introduction

The fog and haze in China continue to increase significantly because of scattered coal burning, straw discharge, and other forms of heating, which are important sources of pollution, particularly in winter, in the Beijing-Tianjin-Hebei region [1,2]. Therefore, searching for a clean alternative energy is imperative. Electricity is a clean energy, and its application is free of pollution, noise, and exhaust gas [3].

The Chinese government implemented the "coal-to-electricity" policy to reduce environmental pollution. The implementation of the policy in the Beijing-Tianjin-Hebei region promotes electric heating. The electricity cost for the valley period is 4.34 cents, which would be reduced to 1.45 cents [4,5] when combined with government subsidies.

However, the large-scale use of electricity increases the negative effect on the power grid during peak periods and enlarges the difference between peak and valley power loads. In addition, although the nighttime electricity load is low in China, power shortages during peak periods have always been a serious problem [6,7]. China continues to exert considerable effort to increase wind power development in Hebei, Zhangjiakou, Inner Mongolia, and other areas. Meanwhile, wind power and electricity demand exhibit a reverse and unstable trend. Therefore, the already significant electricity peak–valley difference in this region will worsen if all areas use wind power [8-10]. According to relevant reports released by national energy administration, the annual abandoned wind power reached 497 billion kWh in 2016. The highest abandoned wind rate observed in Gansu was

*Corresponding author (email: yhzhao29@bjut.edu.cn)

43%, and the lowest abandoned wind rate was 21% [11]. Sufficient storage in a power grid during night valley and daytime peak periods for village building cooling/heating can be used to regulate the grid instead of intermediate and peak generation so that the safety of the grid and the degree of wind power consumption will be improved [12,13].

The development of cold storage technology for cooling has been investigated by many scholars, and many projects have been implemented [14-17]. Although many studies focused on heat storage [18], studies on building heating are relatively rare in China. With regard to storage heating, the application of the electric boiler, which belongs to sensible heat storage (SHS), is relatively common [19]. However, the temperature of SHS materials continuously changes and cannot be maintained at a certain value or range, such that the thermal energy output is unstable and not conducive for use. In addition, the low energy density of SHS results in a large volume of the corresponding device, which is of little value in industrial application [20].

The phase change materials (PCMs) used in latent heat storage (LHS) possess a high storage density and constant temperature during charging and discharging. Therefore, LHS, which requires certain devices, possesses the advantages of reduced size and light weight and exhibits an application potential for thermal energy storage [21,22]. The recent study of latent heat storage was mainly conducted by way of experimental measurement and numerical simulation. Lu et al. [23] studied the heat transfer in molten salt in a cylinder tank via simulation and experiment to obtain its natural convection heat transfer in a single energy storage tank. Shang et al. [24] presented a passive thermal management system (TMS) for downhole electronics by using phase change material and heat pipes, and the thermal characteristics of the TMS was evaluated experimentally. Xia et al. [25] investigated the liquid-solid phase change process of a simple one-dimensional slab and the obtained results can provide some theoretical guidelines for the choice of optimal cooling or heating strategy in practical liquid-solid phase change processes. Zhang et al. [26] proposed a novel non-equidistant helical-coil structure and investigated the heat storage experimentally; furthermore, the structure was optimized using numerical simulation.

Paraffin-type PCMs are commonly used for LHS because of their moderate phase change enthalpy, long-term physical and chemical stability, and repeated phase change, crystallization without the occurrence of subcooling or crystal separation, low vapor pressure, and low cost [27-29].

Investigations on electrical storage heaters using PCMs are relatively scarce and commonly focused on methods using electric heating wires [30,31] or electric heating tubes [32,33]. However, these approaches often lead to high thermal resistance during charging and discharging processes and unstable heat transfer between the heating element and PCM. Moreover, utilizing natural convection heat transfer for indoor heating traps heat and results in an increase in the required PCM temperature. Thus, the application of these storage devices entails a certain risk, and the promotion of heat storage is limited.

Considering these issues, this study used a highly efficient heat transfer component, namely, a flat micro-heat pipe array (FMHPA) [34] with enhanced heat transfer fins, to ensure rapid and efficient heat energy transmission. A novel meso-low-temperature electrical phase change storage heater using #52 commercial paraffin wax was developed, and its thermal characteristics were experimentally investigated. The storage heater exhibited good thermal performance with high thermal efficiency, high energy storage density, and high and relatively stable discharging power.

In the last part of this study, the novel storage heating was hypothetically applied in a rural area in Beijing, China. The costs of direct heating were compared, and the environmental benefits that could be obtained if the energy used for heat storage at night is supplied by wind farms were considered. The results showed that the use of electrical storage heating would provide good economic and environmental benefits.

## 2 Experimental investigation

### 2.1 Details of the experimental setup

An experimental system of the new storage heater based on LHS and FMHPA was designed and used for charging and discharging experiments in an indoor environment. Figure 1 shows the device body and its profile and heat transfer unit diagram. The device has an overall dimension of 729 mm × 581 mm × 201 mm. The experimental setup consisted of the FMHPA assembly, heat storage tank (HST), air duct, support, PCM, and heat insulation material (HIM). A 400-mm-long FMHPA assembly is installed in HST, and a 170-mm-long FMHPA assembly extends out of HST in the air duct and 120 mm into the support. Rubber insulation cotton (50 mm thick) was used as HIM and attached to the outer surface of the device. The HTS, air duct, and support are all made of stainless steel, and the entire device is placed vertically on the ground.

Fifteen FMHPA assemblies were used as a core heat transfer unit. The fins, platen heater, and FMHPA were spliced with thermal silica gel to reduce thermal contact resistance. Number 52 commercial paraffin wax was selected as PCM to store heat in the HST around FMHPA. Aluminum-made equal cross-section rectangular fins were attached to the storage and thermal removal segment with aluminum-made louver fins to achieve heat transfer intensification of the PCM and heat transfer medium (right side of Figure 1). The filling proportion of the cross-section rectangular fins and FMHPAs in HST was 16%.

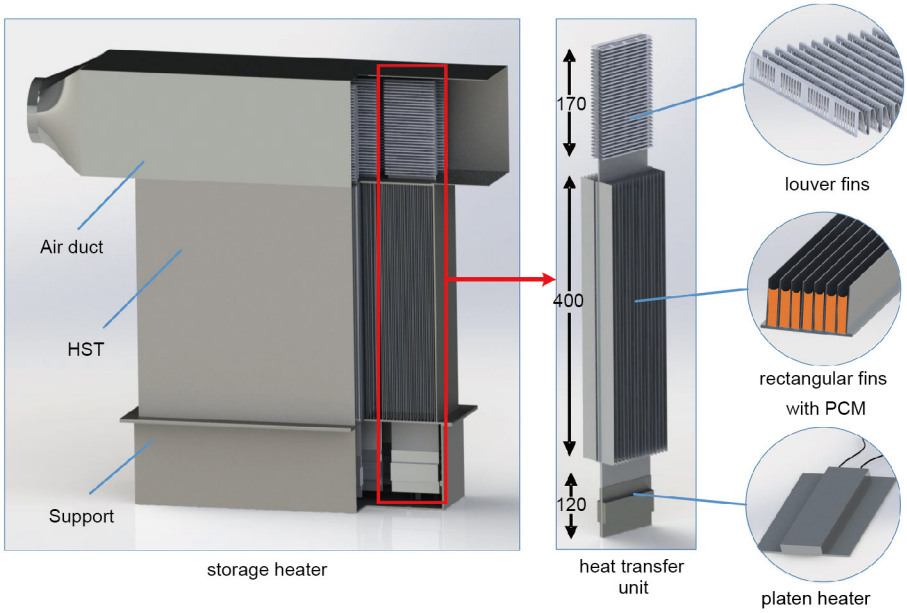


**Figure 1** (Color online) Structure of the storage heater and heat transfer unit.

FMHPA is a heat-conducting member possessing superconducting thermal properties. It has a metal body with a thin plate-like shape and a plurality of independently operated micro-heat pipes arranged inside (Figures 2(b) and 2(c)). Energy transfer occurs during phase change, i.e., evaporation and condensation of the working fluid in the tube. The FMHPA assemblies are divided into three different functional segments from bottom to top according to the working principle. The three segments are heating, thermal storage, and thermal removal, as shown in Figure 2(a). The working fluid in FMHPA is heated and evaporated when the platen heater is energized and vapor is produced up to the thermal storage

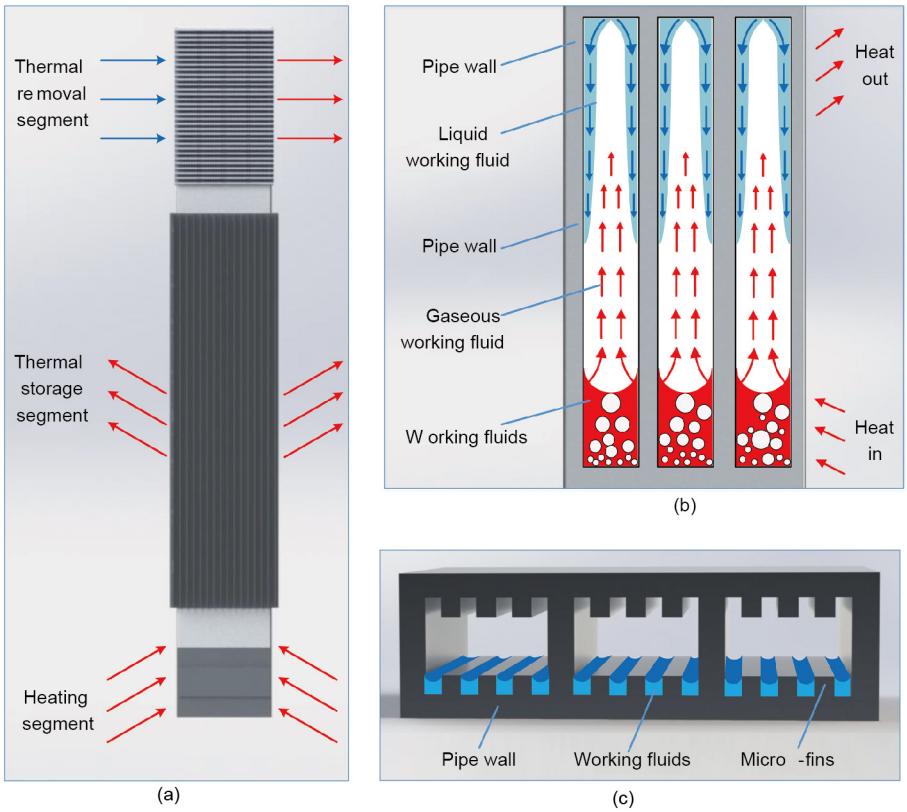


**Figure 2** (Color online) Structure and operating principle of the FMHPA components.

segment. At this point, the working fluid condenses and returns to the heating segment while the energy is transferred to PCM. The charging stage is completed through this cycle. The discharging process is similar to the charging process in that high-temperature PCM heats the thermal storage segment and transfers energy to the thermal removal segment. Meanwhile, air, as the heat transfer fluid (HTF), flows through the air duct, and the energy is released.

The three segments of the device are independent of one another, and the dimensions of the segments can be designed separately. Therefore, the device can be used flexibly for different purposes.

### 2.2 Experimental system

An experimental system for an indoor experiment was set up to test the performance of the new electrical storage heater. The experimental system diagram is shown in Figure 3. The experimental system consists of four main parts: principal experimental part, data acquisition module, cold source, and power control.

The principal experimental part is the storage heater with a PCM mass of 28 kg, and its liquid and solid filling proportions in HST are 81% and 61%, respectively. The thermal-physical properties of #52 commercial paraffin are shown in Table 1.

The cold source includes a water bath, a finned tube air-water heat exchanger, a fan, and a voltage regulator: The voltage regulator controls the fan to change the air volume, and the water bath can provide constant-temperature cold water to the heat exchanger when the air flows through the heat exchanger to the storage air duct.

The power control includes the power supply, voltage regulator, and intelligent power measuring instrument. The voltage regulator is used to adjust the heating power, and the intelligent power measuring instrument [35] is used to record the power consumption and heating power during operation.

The data acquisition module includes a platinum resistance thermometer (model WZPK-293), thermocouples (model WRNK-191), a data collector (model Agilent 34970A; recording time interval of 10 s), a computer, and a flowmeter. The thermal sensor measures the temperature signal through the data collector and transmits the data to the computer. The flowmeter monitors the air volume in the air duct of the storage heater.

### 2.3 Measuring point arrangement

The target temperature was measured by thermocouples, and the thermal resistance of the storage heater during the experiment was arranged at numbers 28 and 8. A 3D coordinate system for the storage heater was established to facilitate the positioning of the measuring point, as shown in Figure 4(a). Fifteen FMHPA assemblies were installed inside the storage heater (3 rows with 5 assemblies each), as shown in Figure 4(b).

Figures 4(c) and (e) illustrate the positions of the thermocouples along the vertical direction of the FMHPA assemblies and the position of thermal resistance in the air duct on the *YZ* plane. TR1–TR4 are located at the inlet of the duct, and TR5–TR8 are located at the outlet of the duct. The temperature inside HTS is symmetrical along the *X*-axis, with the second row of heat pipes (Nos. 6–10) as the symmetry plane. Therefore, the thermocouple inside the box is arranged only

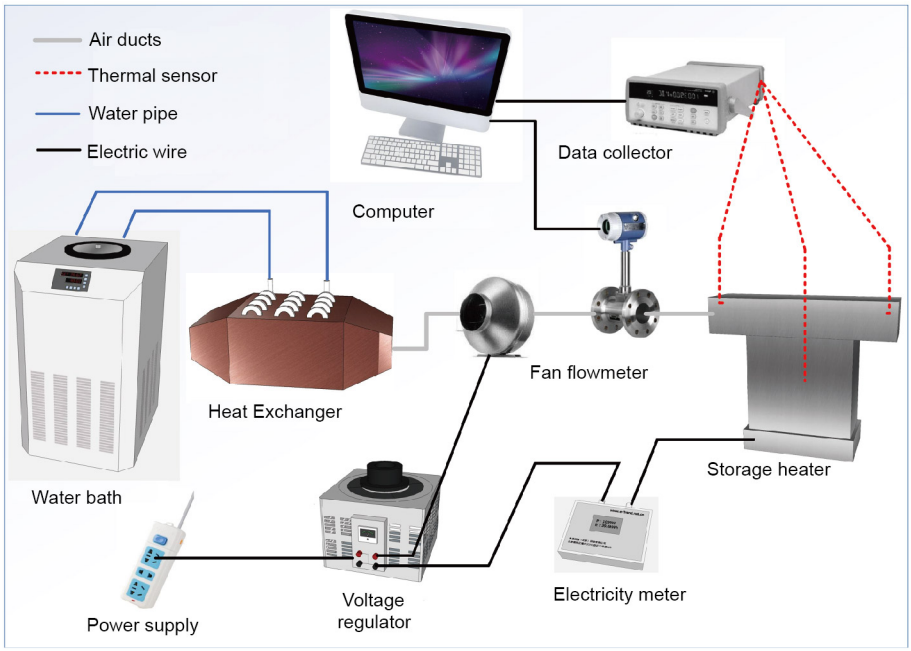


**Figure 3** (Color online) Experimental system diagram.

**Table 1** Thermal-physical properties of #52 commercial paraffin wax

| Parameters | Units | Value |
|---|---|---|
| Phase transition temperature | °C | 52 |
| Latent heat of phase change | kJ/kg | 153.4 |
| Specific heat capacity | kJ/(kg·K) | 2.83 |
| Thermal conductivity | W/m·K | 0.11 |
| Solid-state density | g/cm$^3$ | 1.05 |
| Liquid-state density | g/cm$^3$ | 0.80 |

on one side of the symmetry plane.

Figure 4(d) shows the thermocouple position on the surface of the FMHPA assembly along $X$ and $Z$ directions to test the temperature uniformity of FMHPA during operation.

## 2.4 Experimental condition

The performance of the storage heater was investigated in various working conditions in the charging and discharging processes. The selected PCM temperature range was 35°C to 60°C. The initial temperatures of PCM in the charging and discharging processes were 35°C and 60°C, respectively.

The heating power of the platen heaters was adjusted by the voltage regulator under the charging conditions, which ranged from 202 W to 2044W (followed by 202, 499, 765, 1040, 1322, 1533, 1810, and 2044 W) when the inlet and outlet of the air duct were blocked by an insulation material.

With regard to the discharging conditions, experiments with different air volume flows and inlet temperatures were conducted. The experimental method used was the control variable method that includes constant temperature and constant flow tests (Table 2).

## 2.5 Data analysis

### 2.5.1 *Selection of evaluation indices*

At present, no clear evaluation index is available for thermal storage devices. Therefore, several easy-to-obtain indirect parameters were used in this study. The evaluation indices were selected and calculated as shown below.

Charging/discharging energy:

$$E_{c/d} = M_{PCM}[c_{p,PCM}\left|T_{f,PCM} - T_{i,PCM}\right| + \gamma] + M_{me}c_{p,me}\left|T_{f,me} - T_{i,me}\right|. \quad (1)$$

Average charging/discharging power:

$$\bar{P}_{c/d} = \frac{E_{c/d}}{\Delta t_{c/d}}. \quad (2)$$

Charging efficiency:

$$\eta_c = \frac{E_c}{E}. \quad (3)$$

Extraction energy:

$$E_e = \int_{t_f}^{t_i} \rho_{air} c_{p,air} \dot{q}_{v,air}(T_{out} - T_{in})dt. \quad (4)$$

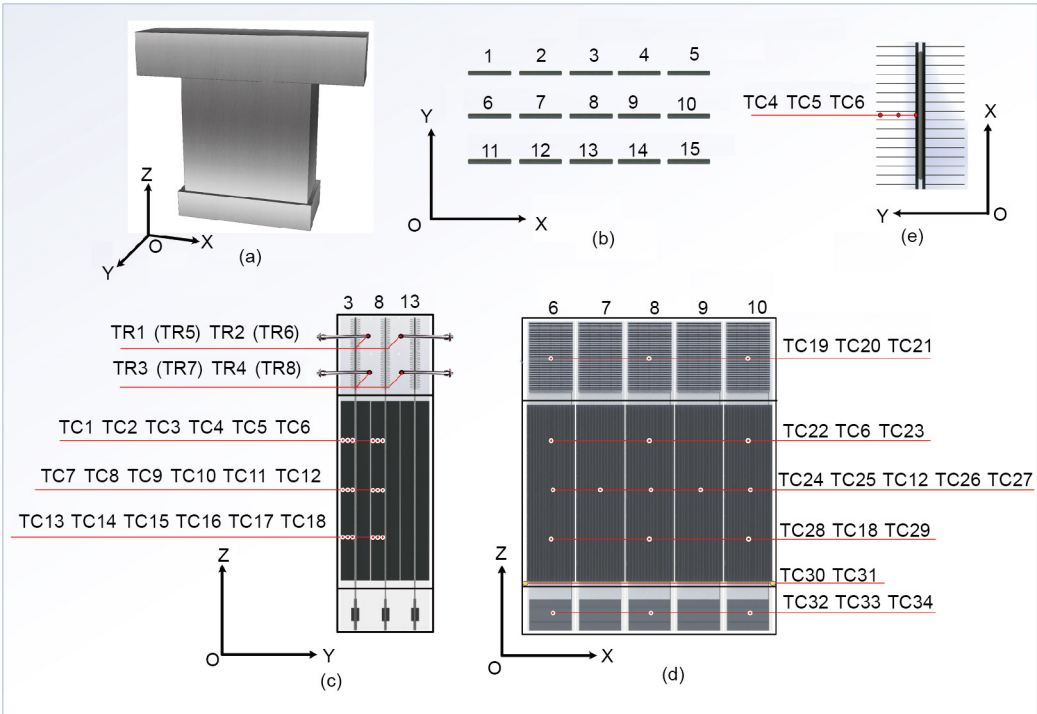


**Figure 4** (Color online) Measuring point arrangement diagram.

**Table 2** Experimental conditions during discharging process

| Experiment | Inlet temperature (°C) | Air volume flow ($m^3$/h) |
|---|---|---|
| Constant temperature test | 15 | 40 |
| | | 60 |
| | | 80 |
| | | 100 |
| | | 120 |
| Constant flow test | 15 | 80 |
| | 18 | |
| | 21 | |
| | 24 | |

Extraction power:

$$\dot{P}_e = c_{p,air}\dot{q}_{v,air}(T_{out} - T_{in}). \tag{5}$$

Extraction efficiency:

$$\eta_e = \frac{E_e}{E_d}. \tag{6}$$

Discharging efficiency:

$$\eta_d = \frac{E_u}{E_d}. \tag{7}$$

In the expressions above, $E_{c/d}$ is the charging/discharging energy of the storage heater (kJ); $M_{PCM}$ and $M_{me}$ are the mass of PCM and metal, respectively (kg); $c_{p,PCM}$ and $c_{p,me}$ are the specific heat capacities of PCM and metal, respectively (kJ/kg·K); $T_{i,PCM}/T_{f,PCM}$ and $T_{i,me}/T_{f,me}$ are the initial and final temperatures of PCM and metal, respectively (°C); $\gamma$ is the latent heat of PCM (kJ/kg); $\overline{P}_{c/d}$ is the average charging/discharging power of the storage heater (W); $\Delta t_{c/d}$ is the time intervals of charging/discharging during the experiment period (s); $\eta_c$ and $\eta_d$ are the charging and discharging efficiencies, respectively (%); $E$ is the electrical energy (kJ); $E_e$ is the extraction energy of the storage heater (kJ); $t_i$ and $t_f$ are the initial and final times during the experiment period (s); $\rho_{air}$ is the air density (kg/$m^3$); $\dot{q}_v$ is the air volume flow ($m^3$/s); $T_{in}$ and $T_{out}$ are the inlet and outlet air temperatures (°C); $\dot{P}_e$ is the instantaneous extraction power (W); $E_u$ is the useful heat consumption to the user (kJ), $E_u = E_e + E_{loss}$ when the storage is used indoors and $E_u = E_e$ when the storage is used outdoors; and $E_{loss}$ is the heat loss of the storage heater (kJ).

The discharging and extraction efficiencies were defined to estimate the thermal efficiency of the storage heater in the discharging process on account of the energy released from the storage heater, which includes heat loss and heat extraction. Moreover, useful heat consumption was considered in accordance with the conditions of use. For instance, heat loss also helps in heating the room if the storage heater is used indoors. Therefore, the discharging efficiency should be 100%, and the useful heat should not contain heat loss if the storage heater is used outdoors; the discharging efficiency should be less than 100% and equal to the extraction efficiency.

### 2.5.2 *Error analysis*

The relative error of the result was determined using independent parameters. If the result $R$ is the relation of independent variables $x_1, x_2, x_3, \ldots, x_n$, such that

$$R = x_1^{a_1} x_2^{a_2} x_3^{a_3}, \ldots, x_n^{a_n}, \tag{8}$$

then the relative error of result $R$ is given as [36]

$$\frac{w_R}{R} = \sqrt{\sum_{i=1}^{n}\left(\frac{a_i w_{xi}}{x_i}\right)^2}, \tag{9}$$

where $w_R$ is the uncertainty of result $R$ and $w_{xi}$ is the uncertainty of the measurement of independent variable $x_i$.

Table 3 shows the model specifications and accuracy of the testing instrument. The thermal-physical properties of PCM or metal are considered constant. Thus, the relative error was calculated with eqs. (1)–(9). The results are listed in Table 4.

## 3 Results and discussion

### 3.1 Temperature distribution of FMHPA assemblies

The FMHPA is the most critical heat transfer element in the storage heater; it directly affects the performance of the storage heater in charging and discharging processes. Figure 5 shows the temperature distribution along the length direction ($Z$ direction) of the No. 8 FMHPA assembly in the charging and discharging processes. The figure also show that the temperature of the thermal storage segment remains uniform and the maximum temperature difference between measuring points on the storage segment under certain conditions during the charging and discharging processes is 3 and 1.5°C, respectively. The experimental results show that

**Table 3** Model specifications and accuracy of the testing instrument

| Testing instrument | Model specification | Accuracy |
|---|---|---|
| Data collector | Agilent 34970A | – |
| Thermocouple | WRNK-191 | ±0.75%\|*t*\|°C |
| Thermal resistance | Pt100 WZPF-293 | 0.15 + 0.2%\|*t*\|°C |
| Flowmeter | TSI-8371 | ±2% |
| Electricity meter | W350 | ±1% |

**Table 4** Uncertainty error of the calculated parameter

| Parameter | Maximum | Unit | Uncertainty |
|---|---|---|---|
| $E_{c/d}$ ($P_{c/d}$) | 7.05 (1.98) | MJ (kW) | ±3.61% |
| $\eta_c$ | 96.97 | % | ±4.13% |
| $E_e$ ($P_e$) | 6.27 (1.41) | MJ (kW) | ±2.29% |
| $\eta_e$ | 86.84 | % | ±4.22% |

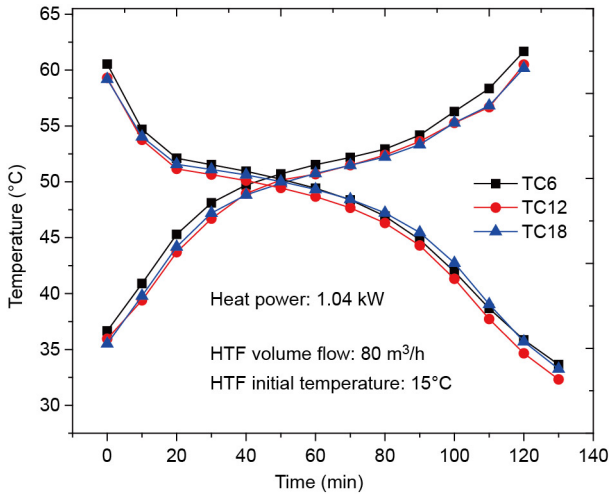


**Figure 5** (Color online) Temperature curve along the *Z* direction of the No. 8 FMHPA assembly versus time in the charging and discharging processes.

the FMHPA has excellent isothermality under the experimental conditions. Thus, energy can be stored and extracted efficiently and rapidly.

Figure 6(a) shows the temperature of Nos. 6–10 FMHPA assemblies at different times in the charging process. Each curve represents the temperature disparities between the assemblies, and the temperature in the *X* direction is more uniform than that in the *Y* direction. The maximum temperature difference of each measuring point is only 1.07°C at 70 min in the charging process. Figure 6(b) exhibits the temperature-time curve along the *X* direction in the discharging process. The difference is that the temperature of each assembly exhibits large divergence, that is, along the direction of HTF. The PCM gradually solidifies because HTF is gradually heated by FMHPA assemblies from the inlet to the outlet, resulting in a large temperature gradient along the *X* direction in the discharging process. These results indicate that this form of heat removal can still be improved, such as by increasing the heat transfer area along the path to improve the temperature uniformity in the *X* direction.

Figure 7 shows the temperature distribution perpendicular to the direction of the No. 8 FMHPA assemblies (TC4–TC6) during charging and discharging processes. The trend is that the farther the distance from the FMHPA assemblies, the lower/higher the temperature of PCM during charging/discharging because the heat flux direction is from PCM to FMHPA assemblies/from FMHPA assemblies to PCM during the charging/discharging process, thus resulting in the occurrence of the abovementioned temperature gradient.

## 3.2 Charging process

### *3.2.1 Electrical energy and PCM temperature variation*

In the experiment, an electric heater was used to supply energy to the heating segment of the FMHPA assemblies and store heat in PCM. As a charging experimental condition, the average temperature range of PCM was 35°C–60°C.

Figure 8 shows the curve of the electrical energy and average temperature of PCM versus time while the heating power is maintained at 1.53 kW (0.10 kW for each FMHPA assembly). The figure shows the rapid warming of PCM at the initial phase of the charging process in the form of SHS. Moreover, the electrical energy curve maintains a linear increase because the heating power remains constant. When heated for about 30 min, the PCM temperature exhibits a gentle curve because the PCM reaches the phase transition temperature and begins to change phase in the form of LHS. Thereafter, the phase change of PCM is completed, and PCM continues to heat up at about 80 min.

In this experimental condition, the total electric energy consumption is 7.24 MJ, which is shown in Figure 9 as the proportion of energy in the form of electrical energy. The charging energy is 7.02 MJ, which accounts for 97% of the total electric energy consumption, scilicet; the charging efficiency is 97%. For the charging completion time of 4720 s, the average charging power is 1.53 kW. In this charging process, 60% of the total heat storage is LHS, which accounts for the largest proportion and improves the energy density of the storage heater significantly. Under the premise of the same stored

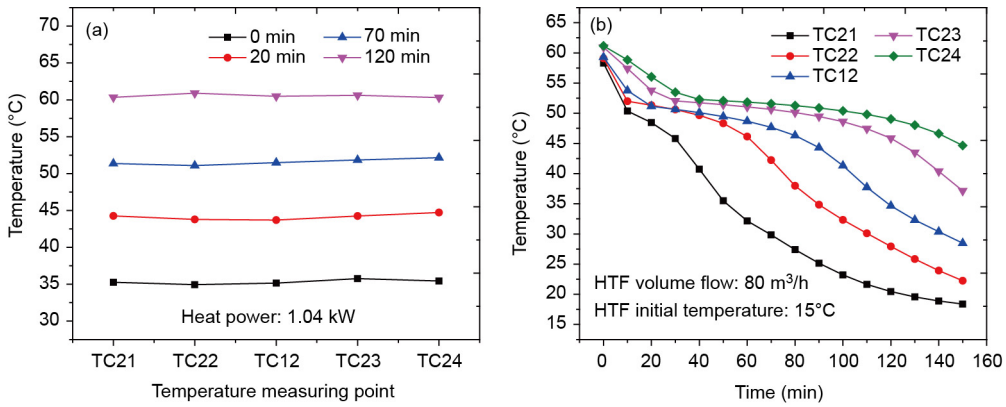


**Figure 6** (Color online) Temperature curves along the *X* direction of Nos. 6–10 FMHPA assemblies at different times in the charging process (a) and versus time in the discharging process (b).

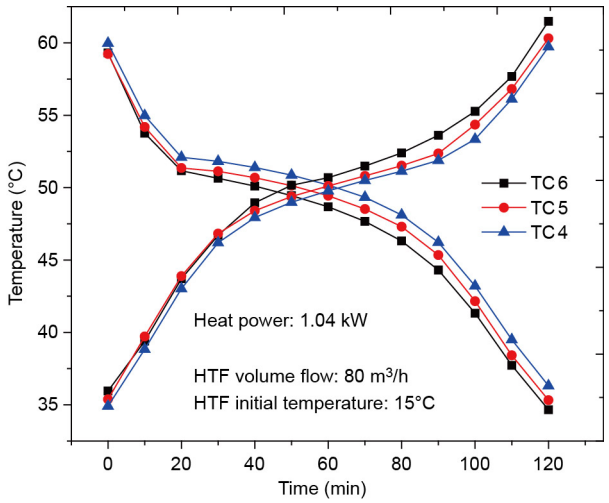


**Figure 7** (Color online) Temperature curve along the *Y* direction of the No. 8 FMHPA assembly versus time in the charging and discharging process.

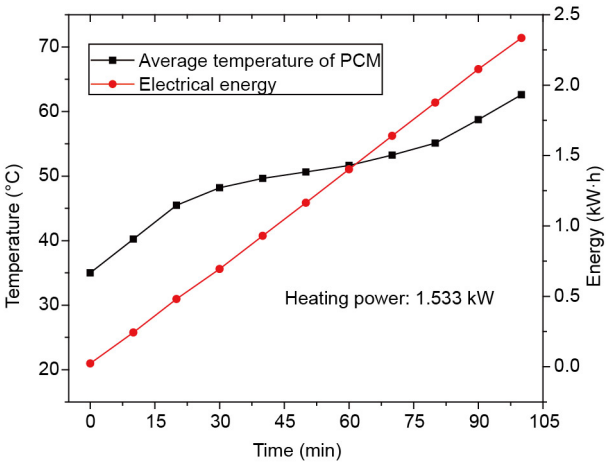


**Figure 8** (Color online) Electrical energy and average temperature of PCM versus time in the charging process.

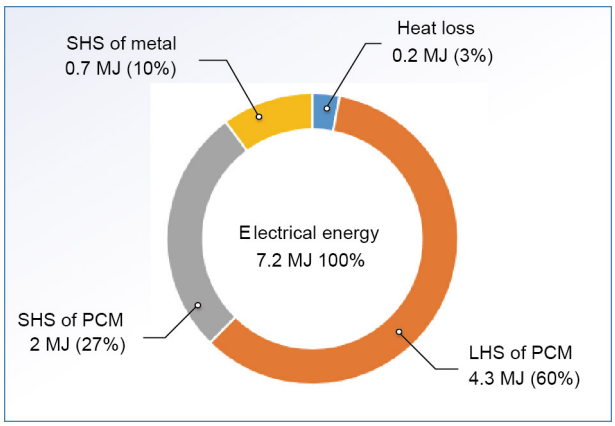


**Figure 9** (Color online) Energy proportion in the charging process.

energy, the PCM temperature is reduced, and effectively improves security.

### 3.2.2 *Effect of the heating power*

The heating power of the regenerative condition is from 0.20–2.04 kW. Figure 10 shows the curve of PCM temperature at different heating powers. With the increase in heating power, the phase change is completed and gradually reaches the set point of 60°C.

Figure 11 shows the charging completion time and efficiency at different heating powers. With the increase in heating power, the charging completion time shortens, and the charging efficiency gradually increases. However, the rate of increase gradually slows down because the longer the charging time is, the longer the time of heat dissipation to the outside of the storage heater is. The maximum heat flux in this research is $1.62 \times 10^4$ W/m$^2$, which is less than the maximum heat flux of FMHPA [37]. Thus, the heat transfer performance of the FMHPA increases with the increase in heating power.

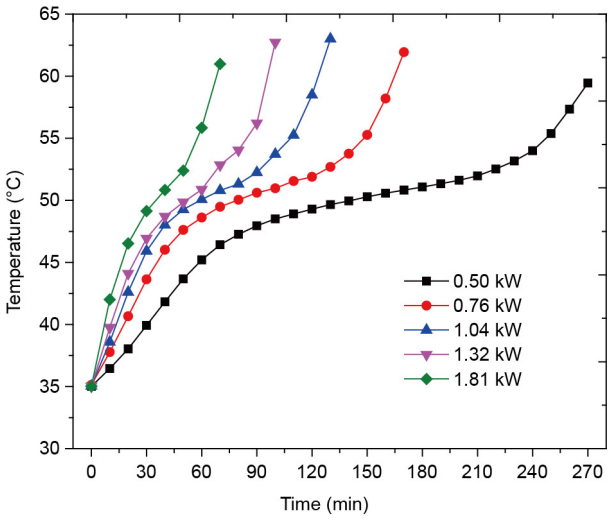


**Figure 10** (Color online) Curve of average temperature of PCM at different heating powers versus time.

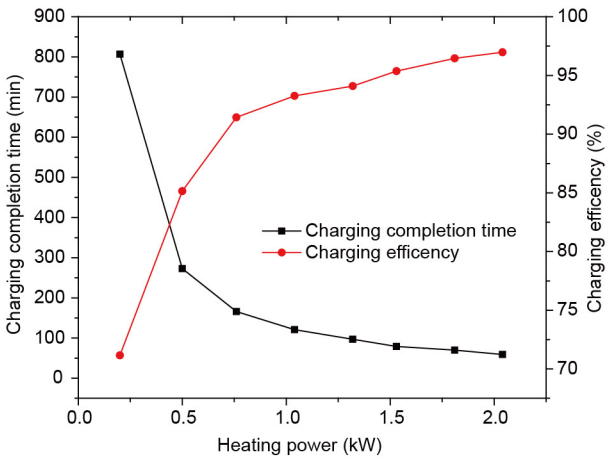


**Figure 11** (Color online) Curve of charging completion time and charging efficiency at different heating powers.

Charging efficiency increases, but the growth rate gradually decreases.

The experimental results obtained during the charging process are as follows. The charging completion times decrease from 806 min to 59 min (approximately 92.68% decrease), and the charging efficiencies increase from 71.16% to 96.97% when the heating power is from 0.20 kW to 2.04 kW. The explanation for the substantial increase in heat storage efficiency is as follows: when the heating power is increased, the temperature of the thermal storage segment of FMHPA assemblies is also increased. Therefore, the temperature difference between PCM and FMHPA increases so that the heat transfer process can be strengthened and the charging rate can be improved. Thus, the storage completion time shortens, and the heat loss of the entire device is reduced. However, the stored energy is basically the same when the charging process is completed. Therefore, the charging efficiency is increased.

Notably, the charging process can proceed at a low level of heating power, i.e., 200 W (13.33 W for each FMHPA assembly), but has a long completion time, i.e., 806 min. This result indicates that when the power supply, e.g., the power generated by wind turbines, is low, the resulting electricity can still be absorbed to a certain extent without being wasted.

### 3.3 Discharging process

#### *3.3.1 Inlet and outlet temperatures of HTF and extraction power*

Air was used as HTF during the discharging process, and indoor air temperature, as the basis for the choice of inlet temperature, was maintained in the range of 15°C–24°C. Figure 12 presents the PCM inlet and outlet temperatures versus time during the discharging process. The inlet temperature and volume flow rate are 15°C and 120 $m^3$/h, respectively. Figure 12 shows that the entire variation trend of PCM and outlet temperature with extraction power is identical and gradual, with an average outlet temperature of 43°C. After about 10 min, the PCM temperature curve becomes gentle and begins to solidify. Thereafter, the phase change is completed at about 60 min. For the discharging completion time of 5280 s, the average discharging and extraction powers are 1.30 and 1.13 kW, respectively. Thus, the extraction and discharging efficiencies are 87% and 100%, respectively.

In this condition, the proportion of the form of energy released from the storage heater is shown in Figure 13. The discharging energy is 6.90 MJ, which includes 62% LHS of PCM to achieve a stable discharging power output. The SHS of PCM also accounts for a relatively large proportion, i.e., 29%, because PCM has a large specific heat capacity. Of the discharging energy, 87% is air-extracted and 13% is lost in the form of heat loss. However, heat loss also helps in indoor heating because the storage heater was tested indoors.

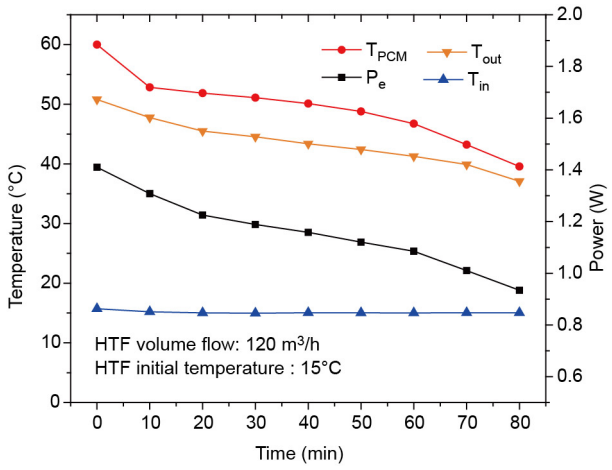


**Figure 12** (Color online) Curve of inlet and outlet temperatures, extraction power and average temperature of PCM versus time.

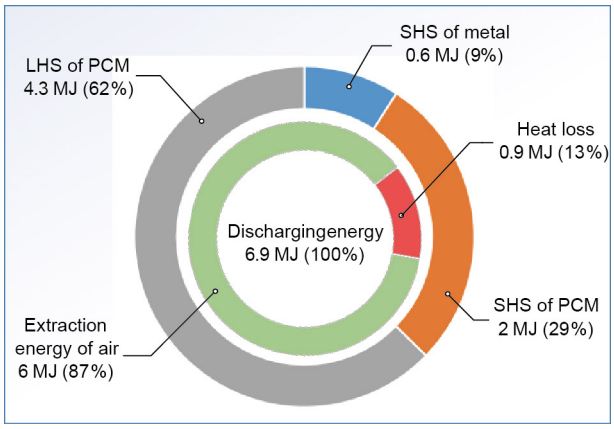


**Figure 13** (Color online) Energy proportion in the discharging process.

#### *3.3.2 Effect of the volume flow rate of HTF*

A fixed inlet temperature with different air volume flow rates was employed to explore the effect of volume flow rate. Figure 14 shows the temperature variation curve of PCM at different volume flow rates of HTF. Volume flow exerts a significant effect on the charging completion time. The volume flow rate is greater, the completion time is shorter. The experimental results are as follows: the discharging completion times are 227, 180, 128, 104, and 88 min when the volume flow rates are 40, 60, 80, 100, and 120 $m^3$/h, respectively; the corresponding decrements are 21%, 44%, 54%, and 61%.

Figure 15 shows the extraction power of air in different volume flow conditions. With the increase in heating power, the extraction power increases because the convective heat transfer coefficient is positively correlated with the velocity of air, i.e., with the increase in volume flow rate, wind speed and extraction power also increase. By contrast, the heat extraction power is stable at a small volume flow rate when heat is conducive to a constant power output. The calculation results are as follows. The average extraction/discharging powers

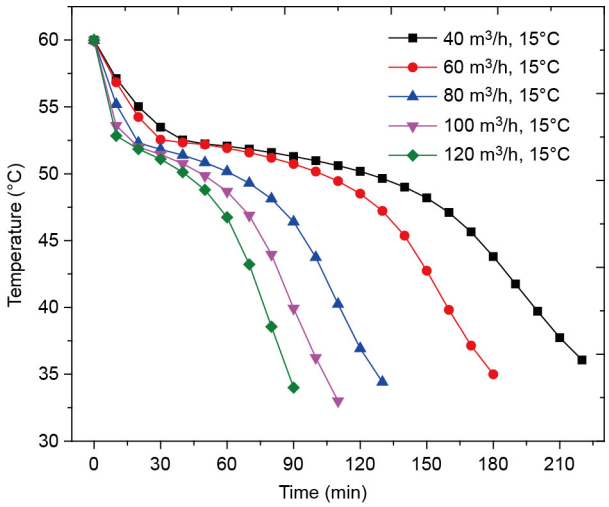


**Figure 14** (Color online) Curve of average temperature of PCM at different volume flow rates of HTF versus time.

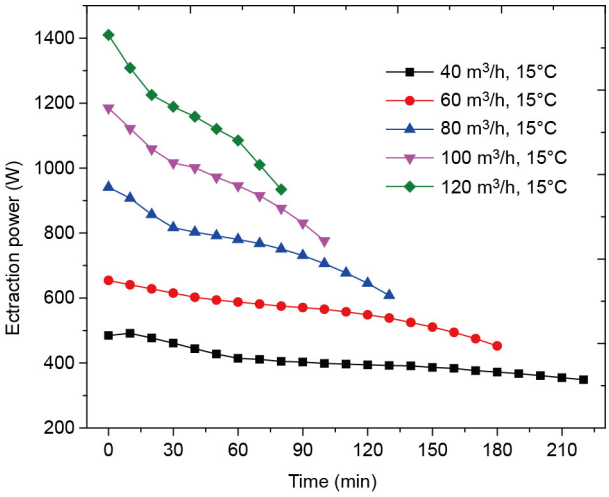


**Figure 15** (Color online) Curve of extraction power at different volume flow rates of HTF versus time.

are 404/512, 551/643, 773/910, 963/1109, and 1126/1298 W when the volume flow rates are 40, 60, 80, 100, and 120 $m^3$/h, respectively; the corresponding increments are 8/59%, 51/125%, 88/175%, and 120/221%.

### 3.3.3 *Effect of the inlet temperature of HTF*

When considering the use of the storage heater, the required room temperature to be maintained is the experimental inlet temperature, i.e., from 15°C–24°C, although high or low inlet temperatures can also be tested. Figure 16 shows the PCM temperature variation curve under different inlet temperatures. The inlet temperature is higher; the discharging completion time is longer. The test discharging completion times are 128, 135, 146, and 167 min when the inlet temperatures are 15°C, 18°C, 21°C, and 24°C, respectively; the corresponding increments are 5%, 14%, and 30%. However, the effect of inlet temperature is not as dramatic as that of the volume flow rate in this test condition.

Figure 17 shows the extraction power of air at different inlet temperatures. The larger the inlet temperature is, the lower the extraction power is because the temperature difference between the evaporation and condensation sections of the heat pipe is an important factor in heat pipe performance. That is, the greater the temperature difference is, the better the heat transfer performance of the heat pipe is. As a consequence, the higher the inlet temperature is, the lower the temperature difference is between the evaporation and condensation sections of the heat pipe and the lower the extraction power is. The calculation results are as follows. The average discharging/extraction powers are 773/910, 704/862, 624/793, and 550/698 W when the inlet temperatures are 15°C, 18°C, 21°C, and 24°C, respectively; the corresponding increments are 9/5%, 19/13%, and 29/23%.

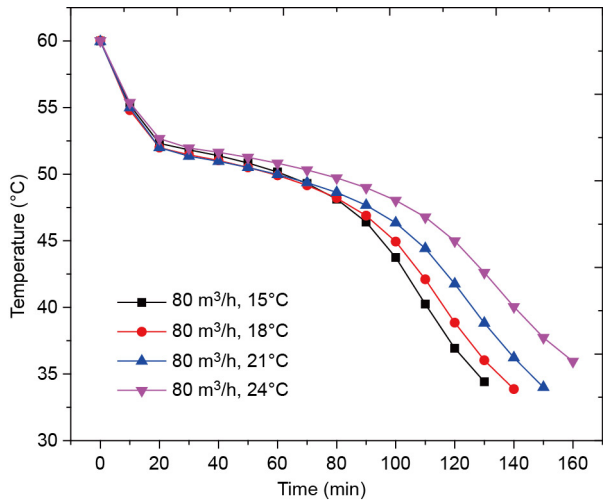


**Figure 16** (Color online) Curve of average temperature of PCM at different inlet temperatures of HTF versus time.

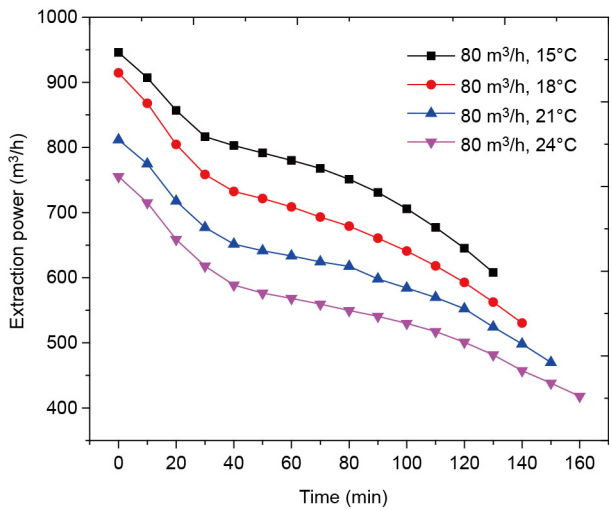


**Figure 17** (Color online) Curve of extraction power at different inlet temperatures of HTF versus time.

### 3.4 Economic and environmental benefits

Coal consumption in rural areas of Beijing accounts for about 60% of the total energy consumption. Scattered coal in the coal consumption structure accounts for 85%. In the vast majority of rural areas that use coal for heating, the heating coal consumption accounts for about 90% of the total coal consumption. The burning efficiency of a civilian small coal stove is only 15%. Coal burning emits dust and other pollutants directly into the atmosphere after combustion, and the intensity of pollutants emitted by coal combustion is 5–10 times the normal power plant emissions [38,39]. The use of clean energy, such as electricity, can significantly reduce the pollution caused by coal combustion heating but will cause new problems. A real-world problem that cannot be solved temporarily is the wastage of the electrical energy generated by power plants because electricity cannot be easily stored. Meanwhile, the electric energy consumption surge and electricity costs are high during the daytime peak period. Utilizing valley electricity to store energy can adjust the peak period of electric energy consumption and protect the safety of the power grid effectively. The policy of the Chinese government, in which the price of electricity differs between peak and valley periods, e.g., the non-valley (06:00–21:00) price is 7.08 cents and the valley (21:00–06:00) price is 1.45 cents after implementing government subsidies promotes the popularization of energy storage heating [40].

In Beijing, the building climate subarea is cold region, and the heating period is from November 15 of the preceding year to March 15 of the subsequent year for a total of 120 days. The application of the proposed device in a 25 $m^2$ house located in a rural area of Beijing was regarded in this study as an example, followed by a simple calculation of the economic and environmental benefits of storage heating. The experimental results show that the charging efficiency of this electrical storage heater can reach 72%–97% when the heating power ranges from 0.2–2 kW and the discharging power reaches 0.5–1.3 kW.

The area heat index of the room was set to 50 W/$m^2$ [41], such that the heating load of the room was 1250 W. A single storage heater can meet the heating requirements of the room. Twenty-four hours of heating, which included 15 h of the non-valley period and 9 h of the valley period, were considered. If a family uses valley electricity to store heat, then the storage heater would heat the room and store energy in the PCM at night. During daytime, the heater heats the room by using the energy stored in the PCM at night.

The electric energy consumption per day for night heat storage is (the considered charging efficiency is 95%)

$$1250\ \text{W} \times 15\ \text{h}/(1000 \times 95\%) = 19.74\ \text{kWh}.$$

Thus, the electric charge per day for night heat storage is

$$19.74\ \text{kWh} \times 1.45\ ¢/\text{kWh} = 28.62\ ¢.$$

If the considered heating efficiency is 100%, then the electric energy consumption per day for night heating would be

$$1250\ \text{W} \times 9\ \text{h}/1000 \times 100\% = 11.25\ \text{kWh}.$$

Thus, the electric charge per day for night heating is

$$11.25\ \text{kWh} \times 1.45\ ¢/\text{kWh} = 16.31\ ¢.$$

Considering that heat has been stored in the PCM at night, only a fan is turned on to extract heat to heat the room. The operating power of the fan is 30 W. Thus, the electric energy consumption per day for daytime heating is

$$30\ \text{W} \times 15\ \text{h}/1000 = 0.45\ \text{kWh}.$$

The electric charge per day for night heat storage is

$$0.45\ \text{kWh} \times 7.08\ ¢/\text{kWh} = 3.19\ ¢.$$

The number of days in the heating season is 120. Thus, the heating cost required for the annual heating season using electrical storage heating is

$$120\ \text{days} \times (28.62 + 16.31 + 3.19)\ ¢/\text{day} = 5774.4\ ¢.$$

If the room is heated by electric heating, then the heating cost required for the annual heating season is

$$120\ \text{days} \times 1.25\ \text{kW} \times (15\ \text{h} \times 7.08\ ¢/\text{kWh} + 9\ \text{h} \times 1.45\ ¢/\text{kWh}) = 17887.5\ ¢.$$

From the point of view of heating cost, the use of storage heating compared with direct electric heating can save 121.12 \$, which can be converted into an area index of 4.85 \$/$m^2$ for the imaginary room.

In the case where the burning efficiency of a civilian small coal stove is 15%, the coal consumption required for heating would be 2948 kgce, which can be converted to an area index of 118 kgce/$m^2$, if the heating method is scattered coal combustion for the annual heating period.

In Beijing, the non-centralized heating area, which mainly involves the use of scattered coal stoves for heating, was 144 $km^2$ by the end of 2012 [42]. By applying the previously presented calculations, $1.699 \times 10^{10}$ kg of standard coal or $2.173 \times 10^{10}$ kWh of electricity is required to heat the non-centralized heating area of Beijing if the heating method is coal stove heating or electrical storage heating. However, the amount of abandoned wind power in China in 2016 was $4.97 \times 10^{11}$ kWh, which is larger than the aforementioned amount. If the main energy source is abandoned wind power, then $1.699 \times 10^{10}$ kg of standard coal can be saved for the annual heating season in Beijing. A saving of one ton of coal may reduce the emissions of $CO_2$ by 2620 kg, $SO_2$ by 8.5 kg, and $NO_x$ by 7.4 kg [43]. A comparison of the pollutant emissions involved in electrical storage heating and coal stove heating is shown in Table 5.

If abandoned wind power in the heating season accounts for one-fourth of the annual abandoned wind power and this electricity is used for all non-centralized heating areas in China

**Table 5** Comparison of the pollutant emissions of electrical storage heating and coal stove heating

| Heating method | Gas | | |
|---|---|---|---|
| | $CO_2$ (kg) | $SO_2$ (kg) | $NO_x$ (kg) |
| Coal stove heating | $4.45 \times 10^{10}$ | $1.44 \times 10^{8}$ | $1.26 \times 10^{8}$ |
| Electrical storage heating | 0 | 0 | 0 |
| Emission reductions | $4.45 \times 10^{10}$ | $1.44 \times 10^{8}$ | $1.26 \times 10^{8}$ |

to supply heat using the method of storage heating, then $1.24 \times 10^{11}$ kWh of abandoned wind power can be saved, which can be converted to $1.52 \times 10^{11}$ kgce of standard coal. If storage heating is promoted nationwide, then it will significantly reduce the heating cost of residents, make full use of the power generated by wind farms, adjust the stability of the grid, and play a good energy-saving emission reduction role.

## 4 Conclusions

Experimental research was conducted to investigate the thermal characteristics of a novel storage heater during charging and discharging processes. An economic and environmental benefit analysis of a hypothetical room was conducted. The following conclusions were obtained.

(1) The FMHPA used in this study showed excellent isothermally under the experimental conditions. The energy can be stored and extracted efficiently and rapidly.

(2) The new storage heater showed a good thermal performance during charging and discharging processes. In the range of the experimental conditions employed in this study, the charging and discharging powers reached 1.98 and 1.30 kW, respectively, and the maximum charging and extraction/charging efficiencies were 97% and 87%/100%, respectively.

(3) With the increase in heating power, the charging completion time decreased and the charging efficiency gradually increased. The charging completion times decreased from 806 min to 59 min (92.68% decrement), and the charging efficiencies increased from 71.16% to 96.97% when the heating power was from 0.20 kW to 2.04 kW. In addition, the storage heater could operate normally under low power.

(4) The higher the volume flow rate of HTF was, the lower the discharging power was and the longer the discharging completion times were. In the experimental conditions, the discharging power increased from 0.51 kW to 1.30 kW (154.90% increment), and the discharging completion time decreased from 227 min to 88 min (61.23% decrement) when the volume rate increased from 40 $m^3$/h to 120 $m^3$/h.

(5) A high inlet air temperature could obtain low discharging powers and long discharging completion times. In the experimental conditions, the discharging power decreased from 0.91 kW to 0.70 kW (23.33% decrement), and the discharging completion time increased from 128 min to 167 min (30.47% increment) when the inlet temperature increased from 15°C to 24°C.

(6) The storage heater can save 4.85 \$/$m^2$ annually if the heating method for the room is storage heating and the storage heating power is direct electric heating. The coal saving is 118 kgce/$m^2$ compared with coal stove heating. The device helps achieve parallel-operated wind power and reduces pollutant emissions.


1 Gao F S. Haze weather, environment and energy: The strategies of HVAC industry (in Chinese). Heat Vent Air Cond, 2013, 9: 33–47
2 Ma X Q, Liu Z, Zhao X Y, et al. The spatial and temporal variation of haze and its relativity in the beijing-tianjin-hebei region (in Chinese). Areal Res Dev, 2016, 35: 134–138
3 Gao Z, Chen D M, Yang J H, et al. Study on rural low-voltage distribution network planning with coal-to-electricity project (in Chinese). Electrotech Electr, 2015, 5: 1–5
4 The Beijing News, 2015. Rural "coal to electricity" subsidies will be unified with the city (in Chinese). http://news.xinhuanet.com/energy/2015-04/06/c_127660081.htm
5 China Economic Net, 2013. 2015 residential electricity will be fully implemented peak and valley price (in Chinese). http://finance.ce.cn/rolling/201312/26/t20131226_1998315.shtml
6 Han D, Cai X G. Short-term scheduling of hydrothermal power system considering environmental protection and time-of-use price (in Chinese). Power Syst Technol, 2009, 14: 78–83
7 Tan Z F, Chen G J, Qi J X, et al. Research on time-of-use price at generation side based on optimal configuration of power resources (in Chinese). Power Syst Technol, 2008, 7: 61–65
8 Pei Z Y, Dong C, Xin Y Z. Review of operation and management of integrating wind power in China (in Chinese). Electr Power, 2010, 11: 20
9 Yang S F. Heat storage system with abandon of a wind power plant in Inner Mongolia (in Chinese). Build Energ Env, 2015, 2: 103–105
10 Pazouki S, Haghifam M R. Optimal planning and scheduling of energy hub in presence of wind, storage and demand response under uncertainty. Int J Electrical Power Energ Syst, 2016, 80: 219–239
11 National Energy Administration, 2016. Wind power grid operation in 2016 (in Chinese). http://www.nea.gov.cn/2017-01/26/c_136014615.htm
12 Dunn B, Kamath H, Tarascon J M. Electrical energy storage for the grid: a battery of choices. Science, 2011, 334: 928–935
13 Blarke M B, Yazawa K, Shakouri A, et al. Thermal battery with CO2 compression heat pump: Techno-economic optimization of a high-efficiency Smart Grid option for buildings. Energ and Buildings, 2012, 50: 128–138
14 Jamieson N V, Sundberg R, Lindell S, et al. Preservation of the canine liver for 24–48 hours using simple cold storage with UW solution. Transplantation, 1988, 46: 517–522
15 Jia J, Wan Y, Shou W W, et al. Ice storage system of China Pavilion in EXPO 2010 (in Chinese). Refrig Air Condit, 2012, 6: 100–103
16 Li G, Hwang Y, Radermacher R. Review of cold storage materials for air conditioning application. Int J Refrigeration, 2012, 35: 2053–2077
17 Sun Y, Wang S, Xiao F, et al. Peak load shifting control using different cold thermal energy storage facilities in commercial buildings: A review. Energ Conv Manage, 2013, 71: 101–114
18 Dinker A, Agarwal M, Agarwal G D. Heat storage materials, geometry and applications: A review. J Energ Institute, 2015, 90: 1–11
19 Gao Y F, Sun Y J. Application of the electric-boiler thermal storage for heating in air-conditioning system (in Chinese). Energ Eng, 2002,

2: 28–31
20 Ip K, Gates J. Thermal storage for sustainable dwellings. In: Proceedings of Sustainable Building, Maastricht, Netherland, 2000
21 Sharma A, Tyagi V V, Chen C R, et al. Review on thermal energy storage with phase change materials and applications. Renew Sustain Energ Rev, 2009, 13: 318–345
22 Al-Abidi A A, Bin Mat S, Sopian K, et al. Review of thermal energy storage for air conditioning systems. Renew Sustain Energ Rev, 2012, 16: 5802–5819
23 Lu Y W, Yu Q, Du W B, et al. Natural convection heat transfer of molten salt in a single energy storage tank. Sci China Technol Sci, 2016, 59: 1244–1251
24 Shang B, Ma Y, Hu R, et al. Passive thermal management system for downhole electronics in harsh thermal environments. Appl Thermal Eng, 2017, 118: 593–599
25 Xia S J, Chen L G, Sun F R. Entransy dissipation minimization for liquid-solid phase change processes. Sci China Technol Sci, 2010, 53: 960–968
26 Zhang G W, Hu P, Liu M H. Thermal performances of non-equidistant helical-coil phase change accumulator for latent heat storage. Sci China Technol Sci, 2017, 60: 668–677
27 Hadjieva M, Kanev S, Argirov J. Thermophysical properties of some paraffins applicable to thermal energy storage. Sol Energ Mater Sol Cells, 1992, 27: 181–187
28 Himran S, Suwono A, Mansoori G A. Characterization of alkanes and paraffin waxes for application as phase change energy storage medium. Energ Sources, 1994, 16: 117–128
29 Alkan C. Enthalpy of melting and solidification of sulfonated paraffins as phase change materials for thermal energy storage. ThermoChim Acta, 2006, 451: 126–130
30 Farid M M, Husian R M. An electrical storage heater using the phase-change method of heat storage. Energ Conv Manage, 1990, 30: 219–230
31 Zhao J, Zhou Z C, Pu Y L, et al. Design and application of electric heating high temperature phase change energy storage device (in Chinese). Agric Eng, 2016, 6: 98–102
32 Wang X, Liu J, Zhang Y, et al. Experimental research on a kind of novel high temperature phase change storage heater. Energ Conv Manage, 2006, 47: 2211–2222
33 Ma G Y, Wang Z H, Yan R S, et al. Making and capability testing of electric heater with phase change accumulator (in Chinese). J Fushun Pet Inst, 2003, 3: 50–53
34 Zhao Y H, Zhang K R, Diao Y H. Heat pipe with micro-pore tubes array and making method thereof and heat exchanging system. U.S. Patent, US20110203777 A1, 2011-8-25
35 Xie J C, Wang Z, Zhou X. Intelligent power measuring instrument (in Chinese). China Patent, CN201773152 U, 2011-3-23
36 Gill R S, Singh S, Singh P P. Low cost solar air heater. Energ Conv Manage, 2012, 57: 131–142
37 Zhao Y H, Wang J Y, Diao Y H, et al. Heat transfer characteristics of flat micro-heat pipe array (in Chinese). CIESC J, 2011, 62: 336–343
38 Chen J H, Bo Y J, Li P S, et al. The emission characteristic of air pollutants from civil furnace in Beijing (in Chinese). In: Proceedings of the 10th National Conference on Atmospheric Environment, Nanning, China, 2003. 303–307
39 Ye J D, Zhang Y J, Jiang J Y, et al. Comparison and analysis about mound coal and raw coal for rural heating (in Chinese). Build Energ Effic, 2016, 11: 102–103
40 Lv K F, Tong L G, Yi S W, et al. Analysis and application of heating control strategy of off-peak electricity heating system (in Chinese). Heat Refriger, 2013, 9: 64–66
41 He P. Heating engineering (in Chinese). 4th ed. Beijing: China Building Industry Press, 2009. 167
42 Qiu J D. Research on rural heating mode (in Chinese). Rural Electrif, 2015, 10: 20–20
43 Zhu T, Zhao Y, Diao Y, et al. Experimental investigation and performance evaluation of a vacuum tube solar air collector based on micro heat pipe arrays. J Cleaner Production, 2017, 142: 3517–3526